Discrete Transfer Cross Section Expansion for Time Dependent Neutron Transport

F. Beranek and R.W. Conn

October 1978
(revised January 1979)

UWFDM-304

Nuc. Sci. and Engr. 71, 100 (1979). January 1979).

FUSION TECHNOLOGY INSTITUTE

UNIVERSITY OF WISCONSIN

MADISON WISCONSIN

Discrete Transfer Cross Section Expansion for Time Dependent Neutron Transport

F. Beranek and R.W. Conn

Fusion Technology Institute
University of Wisconsin
1500 Engineering Drive
Madison, WI 53706

http://fti.neep.wisc.edu

October 1978 (revised January 1979)

UWFDM-304

Nuc. Sci. and Engr. 71, 100 (1979). January 1979).

Discrete Transfer Cross Section Expansion for Time Dependent Neutron Transport

F. Beranek*

E. I. du Pont de Nemours & Co
Savannah River Plant
Aiken, South Carolina 29801

R. W. Conn

Nuclear Engineering Department
University of Wisconsin
Madison, Wisconsin 53706

October 1978

(Revised January 1979)

UWFDM-304

*Research performed while at the University of Wisconsin-Madison

ABSTRACT

A new discrete neutron transfer cross section technique has been developed to resolve difficulties found using the traditional Legendre polynomial expansion for time dependent problems with strong source anisotropy. An important class of such problems is the analysis of blanket performance in inertial confinement fusion systems. The new technique can be readily incorporated without formal changes into existing codes which solve the transport equation. A shielding problem and an ICF blanket problem are used as examples to illustrate both the difficulties presented by the traditional approach and the improvements brought about with the new method.

I. INTRODUCTION

It has been noted previously that the use of a truncated Legendre expansion for the representation of multigroup differential transfer cross sections in combination with a discrete ordinate technique for solving the neutron transport equation often leads to the generation of incorrect (frequently negative) angular fluxes in problems involving severe anisotropies in the source and cross sections. [1-3] Problems of this type include shielding of high energy neutrons and fusion reactor blanket neutronics. Since angular fluxes are usually of no primary interest and the angular integration almost always produces positive scalar fluxes, relatively little effort has been invested in the development of techniques to prevent this error. However, it is found that a conventional time dependent neutronics analysis involving a high energy, anisotropic pulsed source leads to negative scalar fluxes in certain time intervals. These fluxes are not acceptable if one is concerned with instantaneous reaction rates (time dependent reaction rates are important for radiation damage studies of inertial confinement fusion (ICF) reactor blankets). In addition, negative scalar fluxes in steady state problems are found in regions where the source is exclusively due to neutrons reflected from another region (e.g. reflections from a shield).

A partial-range Legendre polynomial cross section expansion was introduced by Attia and Harms[3] to eliminate the possibility of the differential group transfer cross section representation becoming negative over certain angular ranges. This technique in its most general and accurate form is difficult to implement numerically because the wide range of materials and neutron energies prevents the practical selection of any constant set of partial angular ranges. Odom and Shultis[1] describe a method

which closely parallels the technique described in this paper. Their numerical approximation of the transport equation renders the Legendre polynomial expansion unnecessary but requires discrete cross sections for each angular and group transfer. This is the ideal cross section representation for a discrete ordinates solution but it requires the writing of a new numerical code since most present neutron transport codes (e.g. time-dependent ANISN[4] or TIMEX[13]) only accept Legendre polynomial expansion coefficients as input data. The method proposed in this paper is theoretically similar to the Odom and Shultis model but retains the Legendre polynomial formalism. A modification to the data is made such that the discrete cross sections are preserved during the calculation, yet the data can be used by a standard discrete ordinates transport code.

II. THEORY

The neutron transport equation, as presented in Eq. (1), is an integro-differential equation involving seven independent variables,

$$\frac{1}{v}\,\frac{\partial\phi(\vec{r},\vec{\Omega},E,t)}{\partial t} + \vec{\nabla}\cdot D\vec{\nabla}\phi(\vec{r},\vec{\Omega},E,t) + \Sigma_t(\vec{r},E)\phi(\vec{r},\vec{\Omega},E,t) =$$

$$\iint \Sigma_s(\vec{r},E')f(\vec{r};E',\vec{\Omega}' \rightarrow E,\vec{\Omega})\phi(\vec{r},\vec{\Omega}',E't)dE'd\vec{\Omega}' + q(\vec{r},\vec{\Omega},E,t). \quad (1)$$

Several approximations must be made to reduce the equation to a form which is soluble by numerical techniques. For the purposes of this discussion, the time integrated, one-dimensional slab form of Eq. (1) is sufficient;

$$\mu\,\frac{\partial}{\partial x}\,\Phi(x,\mu,E) + \Sigma_t(x,E)\Phi(x,\mu,E) =$$

$$\iint \Sigma_s(x,E')f(x;E',\vec{\Omega}' \rightarrow E,\vec{\Omega})\Phi(x,\mu',E')dE'd\vec{\Omega}' + q(x,\mu,E). \quad (2)$$

II.A. Traditional Approach

The first term on the right hand side of Eq. (2) describes particle scattering from all energy and angular domains of phase space (primed variables) into the region of concern (unprimed variables). Since inelastic scattering is reasonably isotropic, the emphasis is placed on the description of the elastic scattering kernel. The angular dependence of the kernel is often approximated by a Legendre polynomial expansion as

$$\Sigma_{el}(x,E')f_{el}(x;E' \rightarrow E,\mu_o) = \sum_{\ell=0}^{\infty} \frac{2\ell+1}{4\pi}\Sigma_\ell(x;E'\rightarrow E)P_\ell(\mu_o) \qquad (3)$$

where $\mu_o = \vec{\Omega}' \cdot \vec{\Omega}$. Due to the completeness property of Legendre polynomials, the infinite summation is exact when the expansion coefficients are determined using the orthogonality relationship,

$$\Sigma_\ell(x;E'\rightarrow E) = 2\pi\int_{-1}^{1} \Sigma_{el}(x,E')f_{el}(x;E'\rightarrow E,\mu_o)P_\ell(\mu_o)d\mu_o. \qquad (4)$$

The expansion for the scattering kernel can be used in Eq. (2) resulting in

$$\mu \frac{\partial}{\partial x}\Phi(x,\mu,E) + \Sigma_t(x,E)\Phi(x,\mu,E) = \iint \sum_{\ell=0}^{\infty} \frac{2\ell+1}{4\pi}\Sigma_\ell(x;E'\rightarrow E)P_\ell(\mu_o)\Phi(x,\mu',E')dE'd\vec{\Omega}' +$$

$$q(x,\mu,E). \qquad (5)$$

Using the expression $d\vec{\Omega}' = d\mu' d\phi'$ and the addition theorem for Legendre polynomials, the scattering term in Eq. (5) can be easily integrated over the azimuthal direction. The resulting equation is

$$\mu \frac{\partial}{\partial x}\Phi(x,\mu,E) + \Sigma_t(x,E)\Phi(x,\mu,E) = \iint \sum_{\ell=0}^{\infty} \frac{2\ell+1}{2}\Sigma_\ell(x,E'\rightarrow E)P_\ell(\mu)P_\ell(\mu')\Phi(x,\mu',E')dE'd\mu' +$$

$$q(x,\mu,E) \qquad (6)$$

where μ' and μ are the before and after collision direction cosines, respectively.

The energy dependence of the equation is approximated by the multigroup representation and the angular integration is reduced to a weighted summation by the discrete ordinate technique. These procedures are discussed in great detail and appropriate definitions are provided in Ref. (5) so are not elaborated on here. The final form of the transport equation is

$$\mu_j \frac{\partial}{\partial x} \Phi^g(x,\mu_j) + \Sigma_t^g(x)\Phi^g(x,\mu_j) = \sum_{g'=1}^{G} \sum_{\ell=0}^{\infty} \frac{2\ell+1}{2} \Sigma_\ell^{g'\to g}(x) P_\ell(\mu_j) \sum_{i=1}^{N} P_\ell(\mu_i)\Phi^{g'}(x,\mu_i)\omega_i +$$

$$q^g(x,\mu_j) \ . \qquad (7)$$

Within the restrictions imposed by the multigroup and discrete ordinate approximations, this equation is still exact due to the infinite summation over the Legendre polynomial expansion order index. However, as a matter of practicality, this summation must be truncated at some finite limit L. This is the cause of the negative fluxes often observed in discrete ordinate calculations. An upper limit of three is commonly used in fusion neutronics calculations. This figure has been arrived at from steady state sensitivity studies of reaction rates in fusion reactor blankets.[6] It is also this low because of the common misconception that the optimum order of a Legendre polynomial cross section expansion for an N-th order discrete ordinate calculation is either $\leq \frac{N}{2}$ or N-1. As is seen later in this article this is not true for time-dependent and strongly anisotropic problems.

Comparisons of finite order Legendre expansions versus true group transfer cross sections have been illustrated in several references.[1,3,7] The fact that the expansion results in negative values over particular angular ranges and positive values over angular spans where the true cross

section is zero can cause considerable nonphysical distortions of the calculated angular flux. In extreme cases, the scalar flux is negative or definitely incorrect. These extreme cases, however, are important in time dependent calculations and problems involving reflected particles from shielding.

II.B. New Method

The technique we have developed to alleviate these problems involves the application of the multigroup approximation before any treatment of the angular dependence of the scattering kernel. If this is done, the resulting equation is

$$\mu \frac{\partial}{\partial x} \Phi^g(x,\mu) + \Sigma_t^g(x,\mu)\Phi^g(x,\mu) = \sum_{g'=1}^{G} \Sigma_{el}^{g'\to g}(x,\mu_o)\Phi^{g'}(x,\mu')d\vec{\Omega}' + q^g(x,\mu) \quad (8)$$

with the standard multigroup definitions. In addition, the following definition is used:

$$\Sigma^{g'\to g}(x,\mu_o) = \frac{1}{\int_{E_{g'}}^{E_{g'-1}} \Phi(x,\mu',E')dE'} \int_{E_g}^{E_{g-1}} \int_{E_{g'}}^{E_{g'-1}} \Sigma(x,E')f(x;E'\to E,\mu_o)\Phi(x,\mu'E')dE'dE. \quad (9)$$

Using the addition theorem for Legendre polynomials with $\ell=0$, Eq. (8) can be written as

$$\mu \frac{\partial}{\partial x} \Phi^g(x,\mu) + \Sigma_t^g(x)\Phi^g(x,\mu) =$$

$$\sum_{g'=1}^{G} \int\int \Sigma^{g'\to g}(x,\mu\mu'+(1-\mu^2)^{1/2}(1-\mu'^2)^{1/2}\cos(\phi-\phi'))\Phi^{g'}(x,\mu')d\mu'd\phi'+q^g(x,\mu). \quad (10)$$

Allowing the azimuthal dependence to remain continuous but applying the discrete ordinate approximation to the μ variable, Eq. (10) is transformed to

$$\mu_j \frac{\partial}{\partial x} \Phi^g(x,\mu_j) + \Sigma_t^g(x)\Phi^g(x,\mu_j) =$$

$$\sum_{g'=1}^{G} \int \sum_{i=1}^{N} \omega_i \Sigma^{g'\to g}(x,\mu_i\mu_j + (1-\mu_i^2)^{1/2}(1-\mu_j^2)^{1/2}\cos(\phi-\phi'))\Phi^{g'}(x,\mu_i)d\phi' + q^g(x,\mu_j). \quad (11)$$

A code, MGRP, has been written to solve this equation using the discrete transfer cross sections and favorable results were achieved.[1] However, it is of primary importance for the present investigation to develop a procedure which is easily adaptable to existing codes.

This is accomplished by equating the scattering terms in the two equations, Eq. (7) with a finite summation and Eq. (11),

$$\sum_{g'=1}^{G}\sum_{\ell=0}^{L}\frac{2\ell+1}{2}P_\ell(\mu_j)\Sigma_\ell^{*g'\to g}\sum_{i=1}^{N}\omega_i P_\ell(\mu_i)\Phi^{g'}(x,\mu_i) =$$

$$\sum_{g'=1}^{G}\int\sum_{i=1}^{N}\omega_i\,\Sigma^{g'\to g}(x,\mu_i\mu_j+(1-\mu_i^2)^{1/2}(1-\mu_j^2)^{1/2}\cos(\phi-\phi'))\Phi^{g'}(x,\mu_i)d\phi'. \qquad (12)$$

The expansion coefficients on the LHS of Eq. (12) are superscripted with asterisks to indicate that they may be different from the coefficients determined by orthogonality. In order that Eq. (12) be true, the following identity must hold:

$$\sum_{\ell=0}^{L}\frac{2\ell+1}{2}\Sigma_\ell^{*g'\to g}(x)P_\ell(\mu_i)P_\ell(\mu_j)\equiv\int\Sigma^{g'\to g}(x,\mu_i\mu_j+(1-\mu_i^2)^{1/2}(1-\mu_j^2)^{1/2}\cos(\phi-\phi'))d\phi' \qquad (13)$$

If the new expansion coefficients are used as data in a discrete ordinates code, the scattering term of the transport equation is treated as exactly possible within the limits of the discrete ordinate and multigroup approximations. The error introduced by the Legendre polynomial truncation is eliminated.

The last step in this procedure is to determine the new expansion coefficients. Once the quadrature set is chosen the only undetermined value in Eq. (13) is L. It is chosen by requiring that every unique combination of μ_i and u_j is preserved.

The number of unique $\{\mu_i,\mu_j\}$ combinations depends on several factors, namely quadrature order, symmetry conditions, problem geometry and source direction. In order to minimize the expansion order, the usual symmetry conditions are assumed,

$$\sigma(\mu_i \rightarrow \mu_j) = \sigma(\mu_j \rightarrow \mu_i)$$

and

$$\mu_i = \mu_{i+N-1} \cdot$$

This method can also be used with asymmetric quadrature sets but a higher order expansion is then required.

The geometry of the problem influences the value of L. In slab geometry, the one quadrature point of zero weight is ignored. It is however used as a boundary condition in curved geometry. Thus S_N problems in slab geometry require the preservation of cross section only between N quadrature points, i.e.,

$$\begin{aligned} &\sigma(\mu_1 \rightarrow \mu_i) \quad i = 1,2, \ldots, N \\ &\sigma(\mu_2 \rightarrow \mu_i) \quad i = 2, \ldots, N-1 \\ &\sigma(\mu_{\frac{N}{2}} \rightarrow \mu_i) \quad i = \frac{N}{2}, \frac{N}{2}+1 \end{aligned} \quad .$$

This means an S_N calculation requires

$$N + (N-2) + (N-4) + \ldots + 2 = \frac{N(N+2)}{4}$$

cross sections or an expansion order of $L = \frac{N(N+2)}{4} - 1$. However, in curved geometry, the calculation begins with the determination of the angular flux in the weightless direction (usually $\mu_{N+1} = -1.0$). This is then used as a boundary condition to find the solution for the angular flux at μ_N. Therefore, the cross sections $\sigma(-1 \rightarrow \mu_i)$ must be preserved and this adds another N+1 expansion coefficients so that L becomes $\frac{N(N+6)}{4}$.

Similarly, the source direction is important. If a calculation involves a neutron beam normally incident to a surface, it is especially important in time dependent codes to allow the neutrons to travel at $\mu = 1$ (rather than at μ_1 which is slightly off normal) so that the time-space relationship is not destroyed. We do this here by using an analytic first collision source. Even in slab geometry, the preservation of $\sigma(1\rightarrow\mu_i)$ is imperative in order to obtain an accurate first scattered source distribution. In curved geometry, scattering from $\mu = 1$ to $\mu = -1$ should be included due to the boundary condition mentioned earlier. This adds one additional coefficient to the expansion and leads to $L = \frac{N(N+6)+4}{4}$ for an S_N calculation of this nature.

The simplification of $\Sigma^{g'\rightarrow g}(\mu_o)$ is given in Ref. 8 and is not derived here. The result is

$$\Sigma^{g'\rightarrow g}(\mu_o) \equiv \frac{h(\mu_o)}{\Delta g'} \int_a^b dZ\psi(Z)\Sigma(x,Z)f(Z,\eta) \quad , \quad a<b$$
$$\equiv 0 \qquad\qquad\qquad\qquad\qquad\qquad a>b \tag{14}$$

with the definitions

$f(z,\eta) \equiv$ elastic scattering kernel

$\eta \equiv$ cosine of scattering angle in CM system

$$h(\mu_o) \equiv (A+1)^2/[A\Gamma(\mu_o)(\mu_o^2 + A^2 - 1)^{1/2}],$$

$$\Gamma(\mu_o) \equiv \frac{E'}{E} = (A+1)^2/[(A^2-1+\mu_o^2)^{1/2} + \mu_o]^2,$$

$$\Delta g' \equiv \int_{E_{g'}}^{E_{g'-1}} \psi(E')dE' \ ,$$

$\psi(E') \equiv$ energy dependent weighting function,

$a = \max[\Gamma(\mu_o)E_{g+1}; E_{g'+1}]$, and

$b = \min[\Gamma(\mu_o)E_g; E_{g'}]$.

The azimuthal integration is performed in Eq. (13) when the expression for the cross section is substituted from Eq. (14). The resulting algebraic set of L equations and L unknowns is then solved.

A disadvantage of this technique is that the coefficients are dependent upon the quadrature used. Different quadrature sets require different data. However, this problem is relatively minor since many users rely on only one set, often the Gauss quadrature. In any case, any number of data sets can be generated and stored on tape for convenient access.

III. APPLICATION AND RESULTS

III.A. Shielding

A case involving a monodirectional plane source between two parallel slabs (see Fig. 1) is an excellent example to dramatically illustrate the consequences of using a Legendre polynomial cross section expansion. The back scattered neutrons are isolated and the behavior of these neutrons in the absence of an uncollided flux is highlighted in the region behind the source. Simultaneously, the traditional slab problem is examined in slab II enabling one to determine the effect of the alteration of the scattering function on the forward scattered flux.

The slabs are composed of graphite since this material is often associated with fission and fusion reactor designs. It is often considered as a liner and reflector in magnetic confinement fusion reactor designs[9] and as a first wall, reflector and structural material in ICF reactor studies.[10]

The time dependent calculations are performed using the Time-Dependent ANISN (TDA)[11] discrete ordinate computer code. The system is divided into seventeen spatial intervals each of 5 cm width. The number density of

graphite is $5 \times 10^{22}/cm^3$ which implies that the intervals correspond to $\lambda/3$ where λ is the mean free path of a 14 MeV neutron. Time steps are determined such that $\frac{\Delta r}{v\Delta t} = 1$ for first group neutrons ($v = 5.245 \times 10^9$ cm/s). The analytic first collision source option is employed which allows neutrons to be incident normal to the surface of slab II. The magnitude of the source is 3.33×10^9 $s^{-1}cm^{-2}$.

Results for the parallel slab calculations are presented in Figs. 2-9. Note that a circumscribed symbol denotes that the actual calculated value is negative (i.e. Ⓐ = -A). The first five figures depict the results of time dependent calculations using the following five techniques: (1) S_4-P_3 with traditional P_3 expansion; (2) S_8-P_3 with traditional P_3 expansion; (3) S_4-P_8 with traditional P_8 expansion; (4) S_8-P_8 with traditional P_8 expansion; and (5) S_4-P_{11} with new discrete expansion. The last two figures illustrate results of steady state calculations using ANISN. These include results of two other models, the S_{16}-P_3 with traditional expansion and S_4-P_6 with the new discrete expansion. All calculations use Gauss quadrature points and weights.

The temporal distribution of first group neutrons in the fourth spatial interval (middle of slab I) is shown in Fig. 2. Note the large magnitude of the negative reflected flux determined by using a traditional P_3 expansion. The flux determined by using the discrete cross section expansion shows more physically realistic behavior - a small, positive flux due to multiply scattered neutrons. It is shown in Fig. 3 that increasing the order of a traditional expansion (in this case to P_8) causes the calculated flux to approach the magnitude of the discrete expansion flux even though the oscillations and negative values still exist.

There is another important point made by this figure. Contrary to the belief of many users of discrete ordinates codes, increasing the order of the cross section expansion beyond the quadrature order does not imply the retention of superfluous moments. Figures 2 and 3 illustrate this very clearly by the obvious improvement of results when switching from S_4-P_3 to S_4-P_8 techniques. The expansion order should be chosen by sensitivity studies and is dependent on the severity of the anisotropy involved in a problem, not necessarily on the quadrature order.

The next two figures illustrate the effect of the expansion order on the calculation of the flux in slab II, essentially the traditional slab problem. The first group flux in the middle of slab II as determined using the normal P_3 expansion becomes negative at times following the passage of the source pulse. This problem is found regardless of the quadrature order. The use of the discrete expansion generates results which are physically acceptable, a rapid monotonic decline in the flux with time after the source is gone. Fig. 5 illustrates that an increase in the traditional expansion order produces results that coincide with fluxes determined with the new discrete expansion. Note again the dramatic increase in the accuracy of the results found upon switching the calculational model from S_4-P_3 to S_4-P_8.

The spatial profiles of the first group flux at a given time step are exhibited in Figs. 6 and 7. The time chosen corresponds to the time at which

the source pulse is in the middle of slab II. It is briefly noted again that the use of the traditional P_3 Legendre expansion leads to non-physical oscillations in the flux in comparison with the precipitous positive slope predicted using the discrete expansion. Increasing the expansion order reduces but does not eliminate the negative fluxes. Figure 7 may lead one to believe that since the magnitude of the negative flux calculated in slab I is four orders of magnitude less than the flux in slab II, accuracy is insignificant. Note, however, that this flux represents the reflected neutrons that are of primary importance in shielding studies.

The effect of the cross section expansions on steady state (time-integrated) results is illustrated in Figs. 8 and 9. The model again consists of two parallel graphite slabs each 16 cm wide, separated by a 10 cm vacuum region. A plane source emitting neutrons in only one direction is located at the center of the vacuum between the slabs. A uniform spatial mesh with Δx = 2cm is used and the calculation is performed with the ANISN code.

Since time integration has an averaging effect on the fluxes, one notes that the agreement between results using the standard and new techniques is much better than for time dependent problems. The first group fluxes in slab II are identical due to the overwhelming dominance of the pulse. In slab I, however, the nonphysical behavior of the fluxes determined using the P_3 expansion (negative fluxes in the S_4-P_3 case and boundary peaking in the S_{16}-P_3 problem), again appear as they did in the transient example. Allowing for multiple small angle scattering, the use of the new discrete expansion technique yields more physically intuitive results than either of the other methods. Note also that the discrete expansion is a sixth order

expansion since in slab geometry, when the analytic first collision source is not available, transfers between μ_i and ± 1 need not be preserved.

The next figure, Fig. 9, shows the first group angular flux in the middle of slab II (interface between intervals 17 and 18). For illustrative purposes, the P_{11} discrete expansion results are given since the P_6 angular flux is incorrect at $\mu = -1$. The scalar flux calculation is insensitive to this problem since $\mu = -1$ is a weightless direction. Note that the angular flux predicted using the discrete expansion decreases monotonically with the scattering angle while the other angular fluxes oscillate with the general shape of a third order Legendre polynomial.

Time Dependent Reaction Rates

Negative instantaneous neutron damage rates to materials were of great concern at the beginning stages of the laser fusion reactor design program at Wisconsin.[10] The concern was not due exclusively to the fact that the rates were incorrect but also because the effect may propagate through time and cause the integrated damage rates to be incorrect. The results of this research show that the new expansion yields integrated values that are not significantly different from those obtained using the traditional expansion method.

There are two main reasons for this result. One is that the significant negative flux problem resides in the first group. The other groups are affected by the inelastic nuclear downscattering which is predominantly isotropic. Thus even though the first group flux is significantly negative or incorrect, the lower energy group fluxes at early times calculated using a P_3 expansion compare quite well with the results using the new expansion.

At later times, several hundred nanoseconds after a neutron pulse strikes the first wall, all source groups have substantially correct fluxes.

The second cause of the generally good time and energy integrated results is the use of an accurate representation of the neutron source. Although a laser fusion microexplosion may last for just tens of picoseconds, the Doppler broadening of the neutron source energy distribution leads to a time-of-flight spreading in neutron arrival times at the first wall of the reaction chamber. This spreading is further enhanced by neutron moderation within the laser fusion pellet itself. The effectively softer neutron source spectrum which is also spread in time permits one to use a P_3 expansion to solve this problem. Such an approach would not work if the source were completely confined to the highest energy group and the effective source pulse length were essentially zero.

The blanket configuration illustrated in Fig. 10 is used to test the two expansions. Using the softer source spectrum from the pellet, the new expansion leads to only a 2.5% decrease in the total helium production rate in the first wall and a 1.5% increase in the displacements per atom when compared to results from a standard S_8-P_3 computation. The instantaneous damage rates are the same using both data sets until the magnitude of the damage rate reaches levels of less than 1% of the peak rate. At this point the helium production rates dramatically diverge. This is illustrated in Fig. 11 where the abscissa gives the time after the leading edge of the pulse strikes the first wall. The P_3 expansion leads to a relatively large secondary pulse due to reflected high energy neutrons. The new expansion also predicts this but at a much lower level. The displacement rates are

not affected by the change in expansions since the displacement cross section for graphite is large in the low MeV and keV region. Thus, the displacement rate is dominated by source neutrons with energies in these groups which arrive later in time.

IV. CONCLUSIONS

A discrete cross section expansion for use in discrete ordinate neutron transport codes has been found to produce more accurate results than traditional methods in time dependent problems with severe anisotropies on the neutron source or the scattering. A constraint on the technique has been that the representation be easily incorporated into the structure of existing codes with no formal changes necessary.

The technique relies on the fact that the discrete ordinate method utilizes angular transfer probabilities for a finite number of angular combinations. A major characteristic of the new expansion is the preservation of the exact values of the necessary angular scattering cross sections. This is accomplished by determining the required transfer probabilities and generating a set of expansion coefficients which, when used in the code, reproduce the correct cross sections. Since the data retains the formal format of Legendre polynomial cross section coefficients, no code modifications are necessary. Important also is the fact that when the problem does not require such an accurate solution, the P_3 expansion coefficients can be substituted in the traditional manner. In a code written to handle discrete cross sections, this cannot be done since the number of cross sections required is dependent only on the quadrature order.

The new expansion results have been shown to be significantly better than results obtained using traditional methods in the simple parallel slab

problem used to approximate a shielding calculation. This geometry is chosen since the correct behavior of the flux is physically intuitive. Though it may not be absolutely correct, the new expansion leads to results which are better than can be obtained with traditional techniques.

The time dependent damage rates in materials subject to a pulsed neutron source, as in an ICFR, are similar at early times using either expansion method. This is due to source broadening in energy and time which makes the initial anisotropies in the problem less severe.

Acknowledgement

This research has been partially supported by grant ET-77-S-02-4296 from the Office of Laser Fusion, U.S. Department of Energy. We appreciate the detailed comments of one of the reviewers on the importance of multiple small angle scattering.

References

1. J. P. ODOM and J. K. SHULTIS, Nucl. Sci. Eng., 59 (1976) 278.

2. D. H. TIMMONS, Trans. Amer. Nucl. Soc., 16 (1973) 50.

3. E. A. ATTIA and A. A. HARMS, Nucl. Sci. Eng., 59 (1976) 278.

4. W. W. ENGEL, Jr., "A Users Manual for ANISN," Computing Technology Center, Union Carbide Corporation (March 1967).

5. G. I. BELL and S. GLASSTONE, Nuclear Reactor Theory (Van Nostrand Reinhold Co., 1970).

6. M. A. ABDOU, "Calculational Methods for Nuclear Heating and Neutronics and Photonics Design for CTR Blankets and Shields," Ph.D. Thesis, University of Wisconsin (1973).

7. H. BROCKMANN, 8th SOFT, Noordwigerhaut, The Netherlands (1974) 949.

8. W. J. MIKOLS and J. K. SHULTIS, Nucl. Sci. Eng., 62 (1977) 738.

9. B. BADGER, et al., "UWMAK-II, A Conceptual D-T Fueled Helium Cooled Tokamak Power Reactor Design", Nuclear Engineering Dept. Report UWFDM-112, University of Wisconsin (Sept. 1975).

10. R. W. CONN, et al., "SOLASE - A Conceptual Laser Fusion Reactor Design", Nuclear Engineering Dept. Report UWFDM-220, University of Wisconsin (Dec. 1977).

11. S. A. DUPREE, et al., "Time Dependent Neutron and Photon Transport Calculations Using the Method of Discrete Ordinates," Joint Los Alamos Scientific Laboratory - Oak Ridge National Laboratory Report LA-4557 (ORNL-4662) (1971).

12. F. BERANEK, "Time Dependent Neutronics Studies in Inertial Confinement Fusion", Ph.D. Thesis at the University of Wisconsin (1978).

13. W. H. REED, "TIMEX: A Time-Dependent Explicit Discrete Ordinates Program for the Solution of Multigroup Transport Equations", Los Alamos Scientific Laboratory Report LA-4800 (1972).

Table 1

Neutron 25 Energy Group Structure in eV Group Limits

Group	E(Top)	E(Low)	E(Mid Point)
1	1.4918 (+7)	1.3499 (+7)	1.4208 (+7)
2	1.3499 (+7)	1.2214 (+7)	1.2856 (+7)
3	1.2214 (+7)	1.1052 (+7)	1.1633 (+7)
4	1.1052 (+7)	1.0000 (+7)	1.0526 (+7)
5	1.0000 (+7)	9.0484 (+6)	9.5242 (+6)
6	9.0484 (+6)	8.1873 (+6)	8.6178 (+6)
7	8.1873 (+6)	7.4082 (+6)	7.7979 (+6)
8	7.4082 (+6)	6.7032 (+6)	7.0557 (+6)
9	6.7032 (+6)	6.0653 (+6)	6.3843 (+6)
10	6.0653 (+6)	5.4881 (+6)	5.7787 (+6)
11	5.4881 (+6)	4.4933 (+6)	4.9907 (+6)
12	4.4933 (+6)	3.6788 (+6)	4.0860 (+6)
13	3.6788 (+6)	3.0119 (+6)	3.3453 (+6)
14	3.0119 (+6)	2.4660 (+6)	2.7390 (+6)
15	2.4660 (+6)	1.3534 (+6)	1.9097 (+6)
16	1.3534 (+6)	7.4274 (+5)	1.0481 (+6)
17	7.4274 (+5)	4.0762 (+5)	5.7518 (+5)
18	4.0762 (+5)	1.6573 (+5)	2.8667 (+5)
19	1.6573 (+5)	3.1828 (+4)	9.8779 (+4)
20	3.1828 (+4)	3.3546 (+3)	1.7591 (+4)
21	3.3546 (+3)	3.5358 (+2)	1.8541 (+3)
22	3.5358 (+2)	3.7267 (+1)	1.9542 (+2)
23	3.7267 (+1)	3.9279 (+0)	2.0597 (+1)
24	3.9279 (+0)	4.1399 (-1)	2.1718 (+0)
25	4.1399 (-1)	2.200 (-2)	2.1800 (-1)

Figure Captions

Fig. 1 Model problem of two parallel slabs with a plane source in the vacuum emitting neutrons only in the direction of slab II.

Fig. 2 First group flux vs. time in interval 4 of ^{12}C reflecting slab system (S_4P_3, S_8P_3, S_4P_{12}). The density factor on this and subsequent figures is a constant which multiplies the actual atomic density and is used to account for voids, porosity, coolant channels or other features which may lower the density of an homogenized zone below the actual physical density.

Fig. 3 First group flux vs. time in interval 4 of ^{12}C reflecting slab system (S_4P_8, S_8P_8, S_4P_{12}).

Fig. 4 First group flux vs. time in interval 12 of ^{12}C reflecting slab system (S_4P_3, S_8P_3, S_4P_{12}).

Fig. 5 First group flux vs. time in interval 12 of ^{12}C reflecting slab system (S_4P_8, S_8P_8, S_4P_{12}).

Fig. 6 First group flux vs. interval in ninth time step ^{12}C reflecting slab system (S_4P_3, S_8P_3, S_4P_{12}).

Fig. 7 First group flux vs. interval in ninth time step in ^{12}C reflecting slab system (S_4P_8, S_8P_8, S_4P_{12}).

Fig. 8 Steady state first group flux vs. interval in ^{12}C reflecting slab system (S_4P_3, $S_{16}P_3$, S_4P_6).

Fig. 9 First group angular fluxes in middle of slab (S_4P_3, $S_{16}P_3$, S_4P_{12}).

Fig. 10 Blanket schematic for ANISN and TDA studies.

Fig. 11 Instantaneous helium production rate in first wall at late times (normal P_3 vs. new P_{12} expansions).

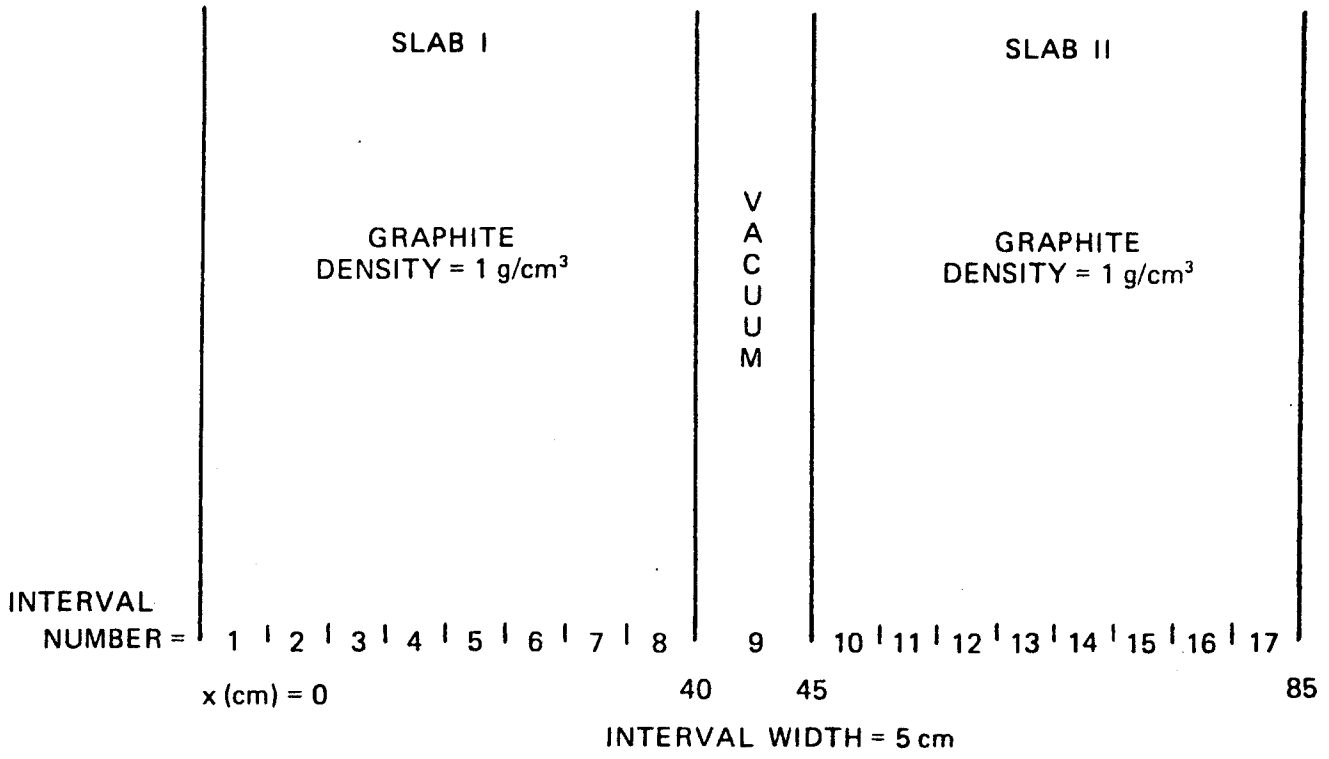

Figure 1

SCALAR FLUX IN INTERVAL 4
○ = NEGATIVE VALUE
A = S_4P_3 TRADITIONAL
B = S_8P_3 TRADITIONAL
C = S_4P_{12} NEW
MATERIAL: ^{12}C
DENSITY FACTOR: 0.05
ENERGY GROUP: 1

Figure 2

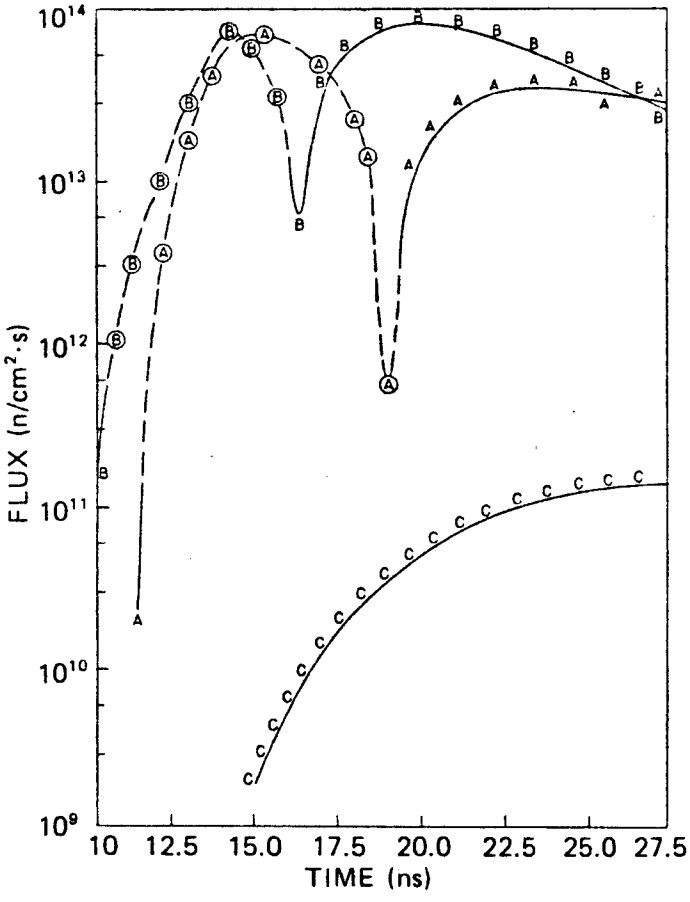

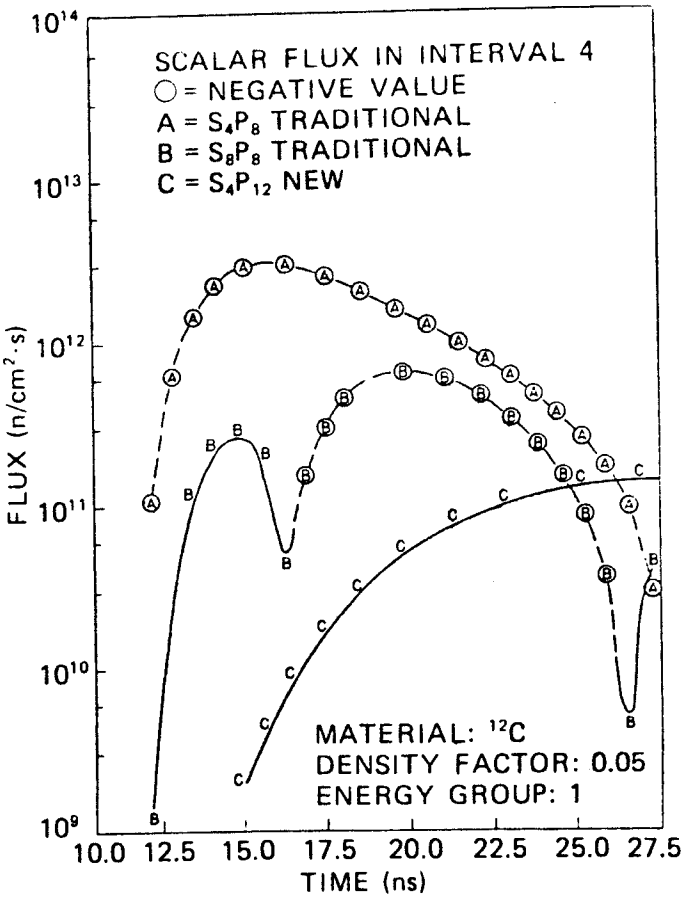

Figure 3

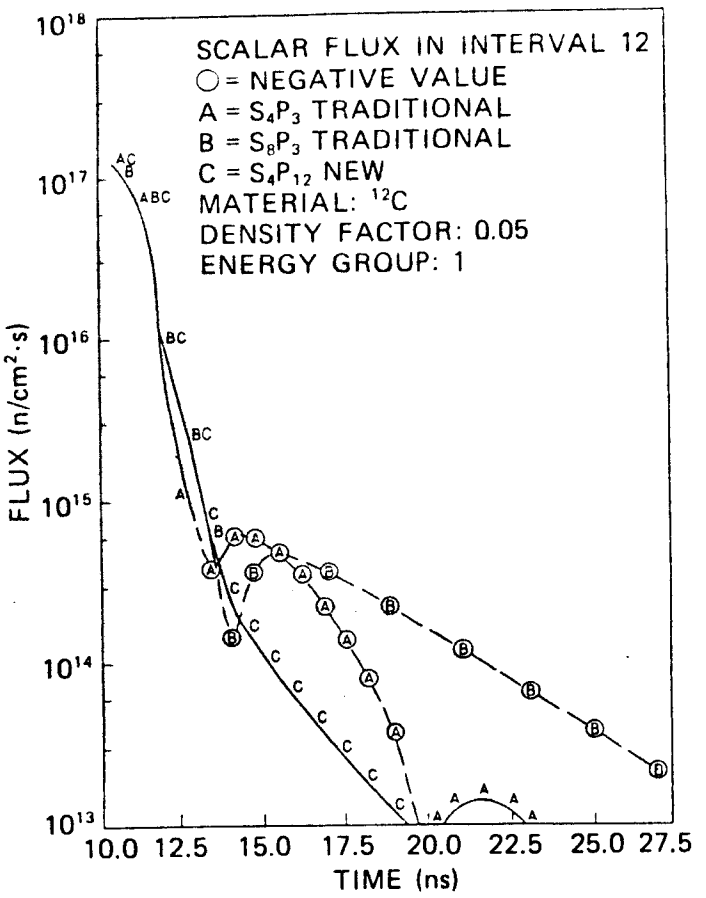

Figure 4

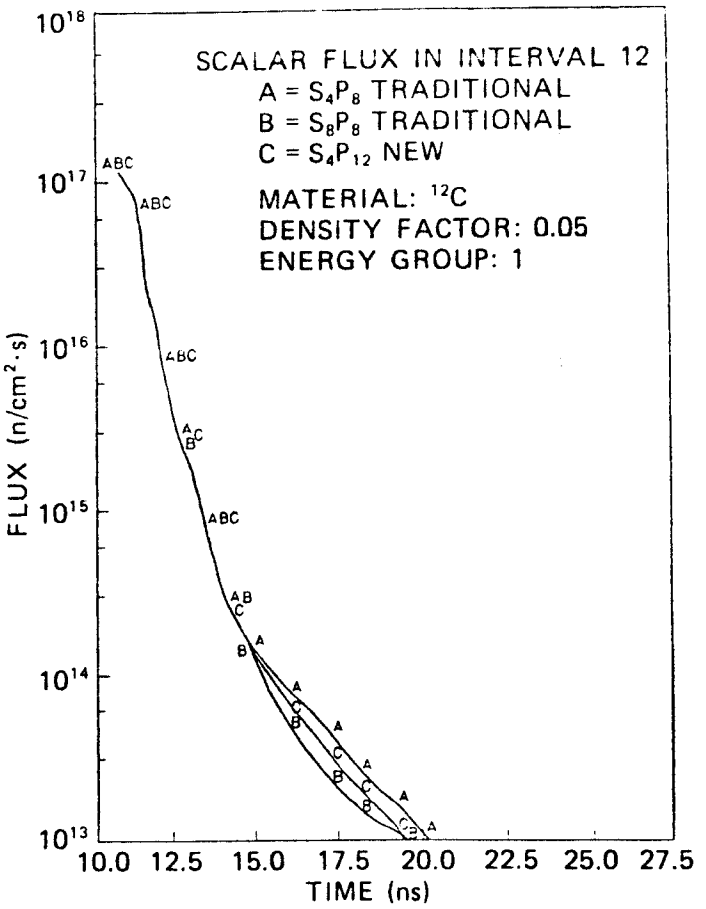

Figure 5

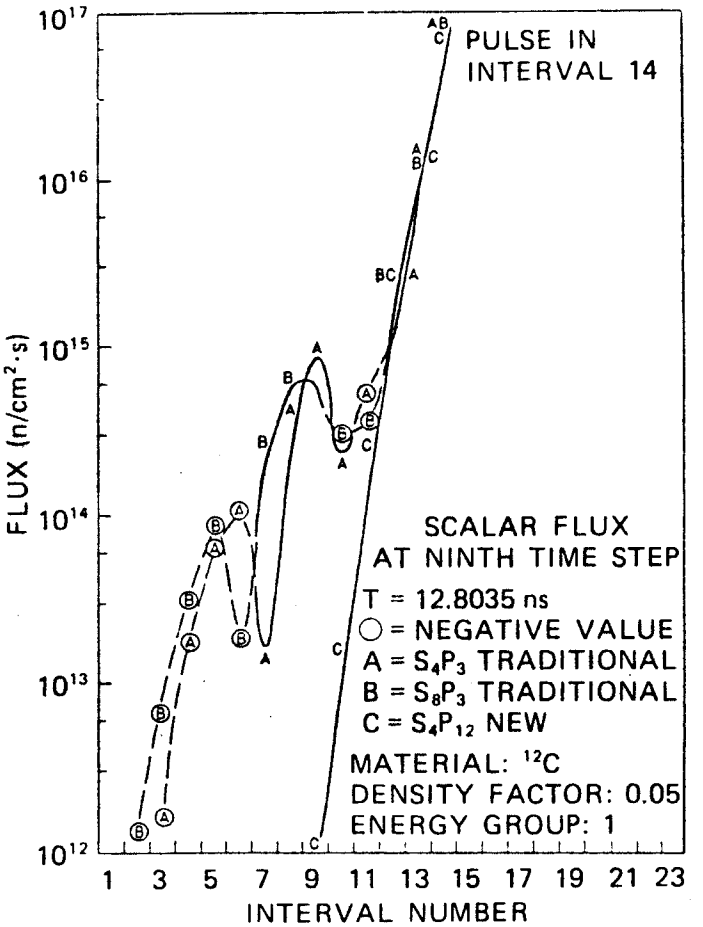

Figure 6

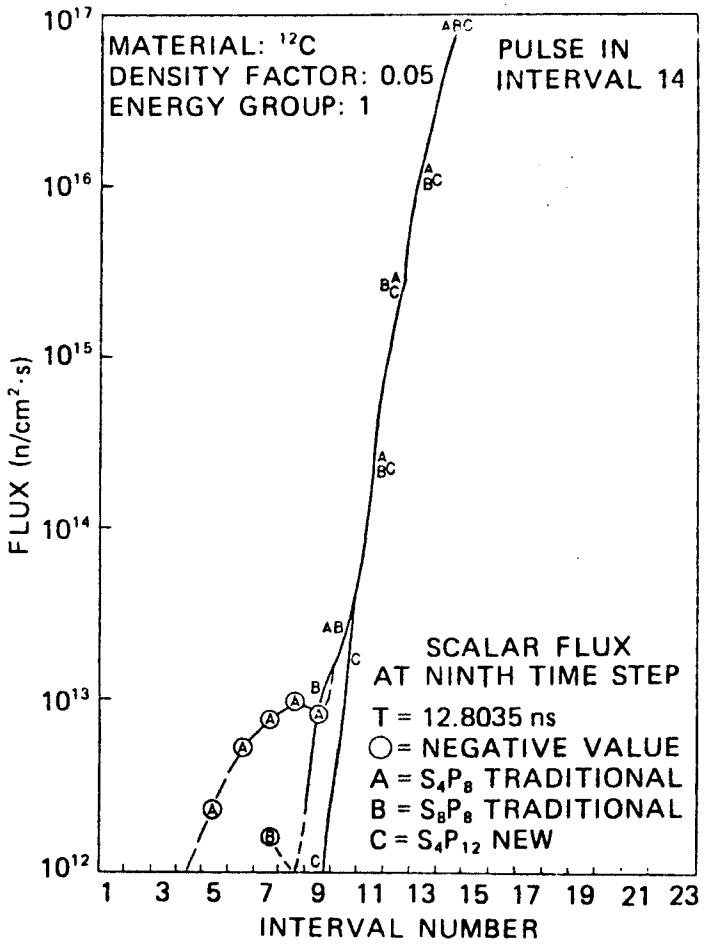

Figure 7

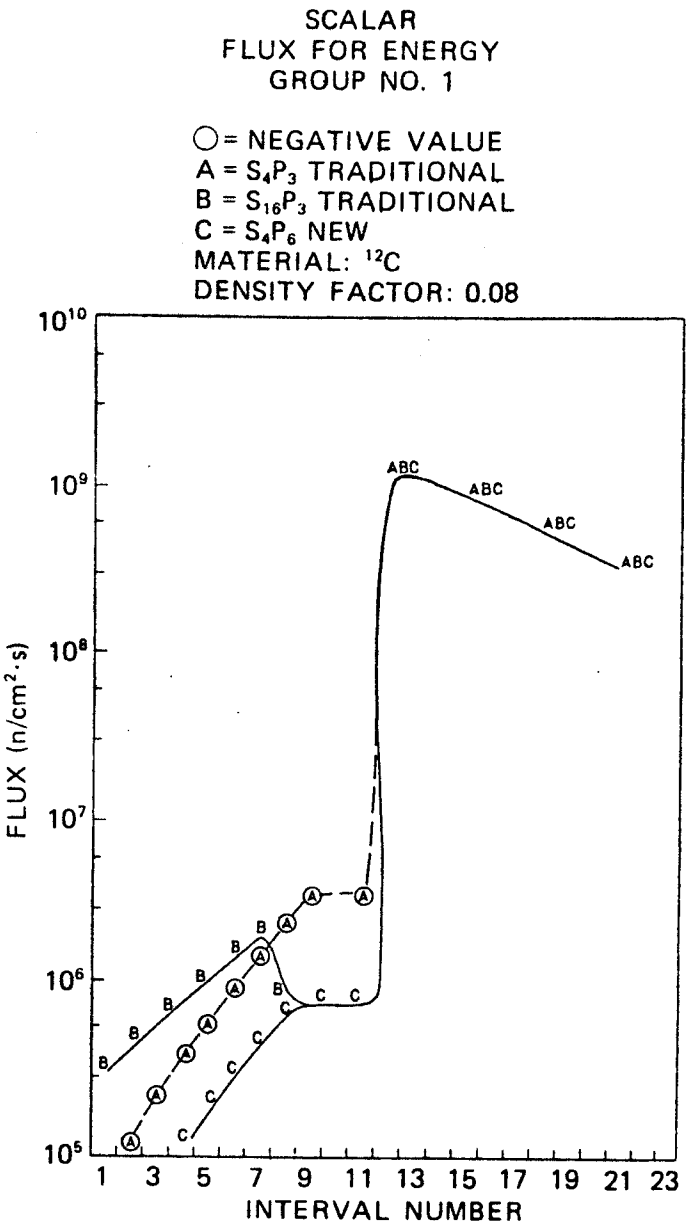

Figure 8

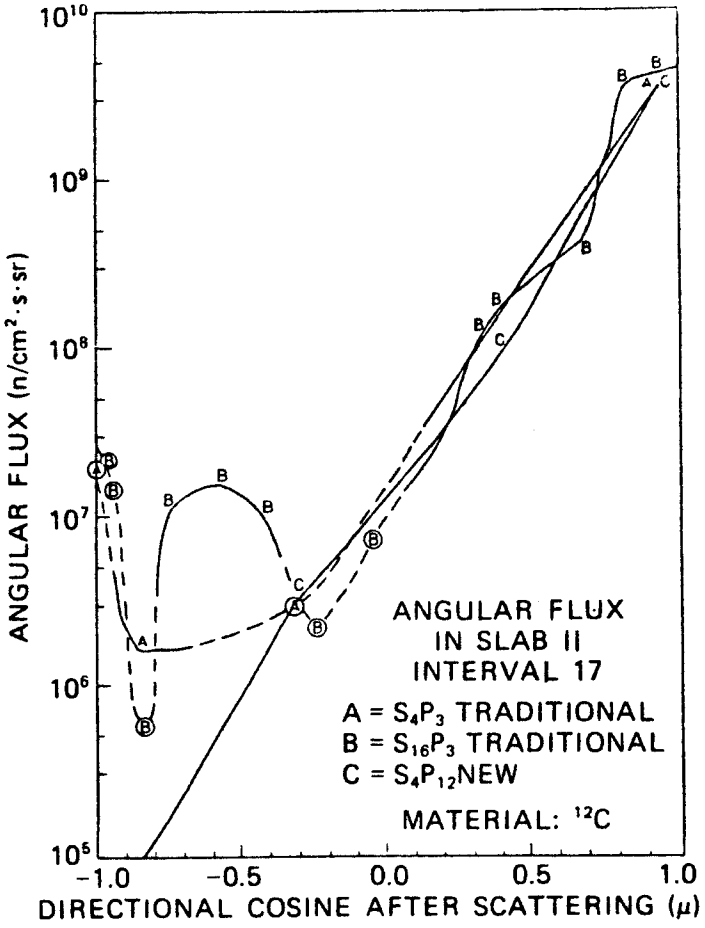

Figure 9

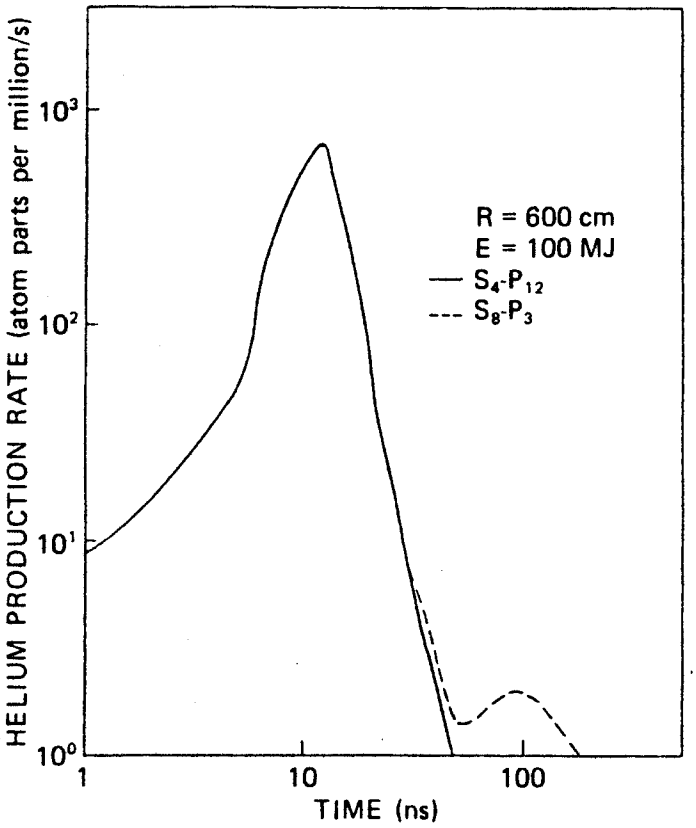

Figure 11

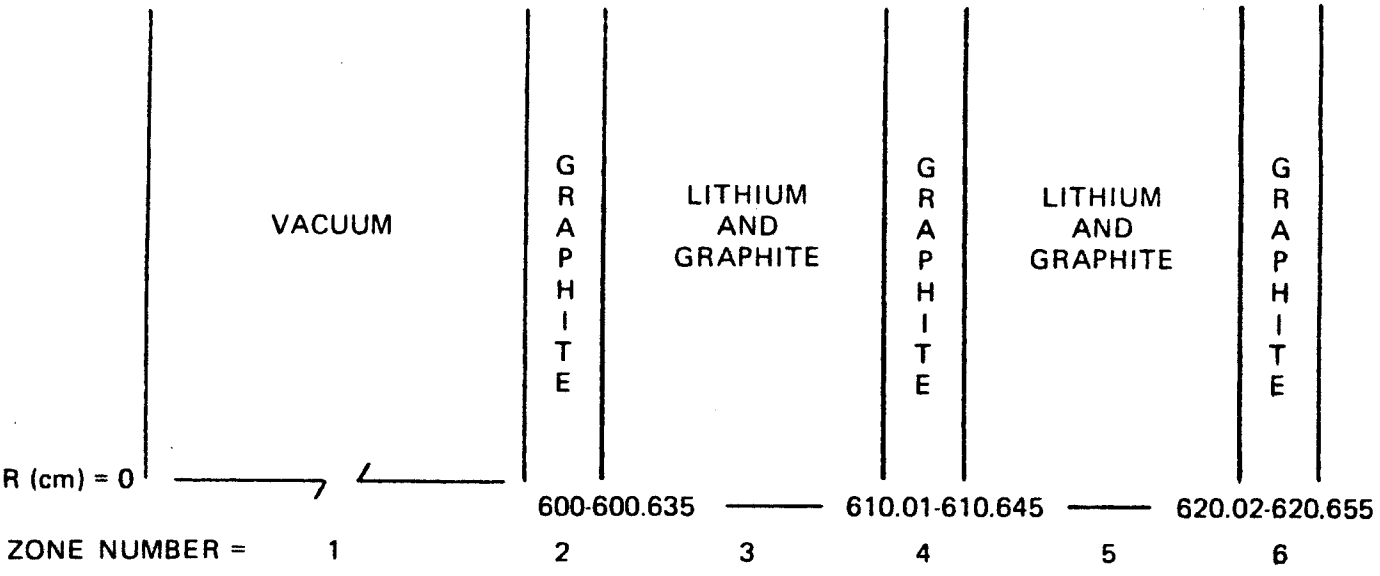

DENSITY FOR ZONES 2,4,6: $^{12}C = 0.048138 \times 10^{24}$ atom/cm^3
DENSITIES FOR ZONES 3,5: $^{12}C = 0.001444 \times 10^{24}$,
$^{6}Li = 0031 \times 10^{24}$, $^{7}Li = 0.0389 \times 10^{24}$ atom/cm^3
GEOMETRY: SPHERICAL

Figure 10